www.czasopisma.pan.pl PAN POLSKA AKADEMIA NAUK www.journals.pan.pl

A R C H I V E S O F M E T A L L U R G Y A N D M A T E R I A L S

Volume 59 2014 Issue 3

DOI: 10.2478/amm-2014-0203

A. GRAJCAR*, M. RÓŻAŃSKI**, M. KAMIŃSKA***, B. GRZEGORCZYK*

STUDY ON NON-METALLIC INCLUSIONS IN LASER-WELDED TRIP-AIDED Nb-MICROALLOYED STEEL

BADANIA WTRĄCEŃ NIEMETALICZNYCH W SPAWANEJ LASEROWO STALI TRIP Z MIKRODODATKIEM Nb

The work concerns the studies on non-metallic inclusions occuring in laser-welded Si-Al TRIP steel containing Nb and Ti microadditions. Laser welding tests of 2 mm thick thermomechanically rolled sheets were carried out using keyhole welding and a solid-state laser. The results of laser welding in the air atmosphere for the heat input value of 0.048 kJ/mm are included. The distribution, type and chemical composition of non-metallic inclusions formed in the base metal, heat-affected zone, and fusion zone are analysed in detail. It was found that the base metal contains rare, fine oxysulphides. Their chemical composition was modified by rare earth elements. Numerous oxide inclusions of a various size and a chemical composition occur in the fusion zone. The dependence between a size of particles and their chemical composition was observed. A microstructure of steel was assessed using light microscopy and scanning electron microscopy techniques.

Keywords: TRIP steel, non-metallic inclusions, laser welding, multiphase microstructure, retained austenite, fusion zone, heat-affected zone

Praca dotyczy badań wtrąceń niemetalicznych występujących w przetapianej laserowo stali TRIP typu Si-Al zawierającej mikrododatki Nb i Ti. Próby spawania laserowego odwalcowanych termomechanicznie taśm o grubości 2 mm przeprowadzono z wykorzystaniem lasera na ciele stałym i techniki głębokiego przetopienia. Przedstawiono wyniki przetapiania laserowego próbek z energią liniową 0.048 kJ/mm w atmosferze powietrza. Szczegółowej analizie poddano rozkład, rodzaj i skład chemiczny wtrąceń niemetalicznych tworzących się w materiale rodzimym, strefie wpływu ciepła i strefie przetopionej. Stwierdzono, że w materiale rodzimym występują nieliczne, drobne wtrącenia siarczkowo-tlenkowe, których skład chemiczny został zmodyfikowany przez pierwiastki ziem rzadkich. W strefie przetopionej występują liczne wtrącenia tlenkowe o zróżnicowanej wielkości i składzie chemicznym. Zaobserwowano zależność między wielkością wtrąceń a ich składem chemicznym. Mikrostrukturę stali określono z wykorzystaniem mikroskopii świetlnej i skaningowej mikroskopii elektronowej.

1. Introduction

Mechanical properties and formability of Advanced High Strength Steels (AHSS) dedicated for the automotive industry are dependent on relative amounts and properties of individual microstructural constituents. Dual phase and multiphase sheet steels containing retained austenite are grades of special interest due to their superior combination of high strength and ductility [1-4]. The final mechanical properties of the latter group showing transformation incuced plasticity effect are formed during forming under conditions of strain-induced martensitic transformation of metastable retained austenite [4-7]. Generally, these are C-Mn-Si, C-Mn-Al or C-Mn-Si-Al steels with a typical content of 1.5% Mn and 1.7% (Si+Al). Silicon and aluminium are needed to prevent carbide precipitation and hence austenite retention during isothermal holding of steel in a bainitic transformation range. The Al-bearing steel grades are characterized by lower strength levels compared to Si-containing steels. Therefore, C-Mn-Al steel grades contain increased up to about 0.3% C content. Due to weldability requirements the decrease in strength can be better compensated by Nb/Ti/V microalloying [7-9] similarly to its beneficial effect in fine-grained HSLA steels [10-13]. These steel grades can be produced both as cold-rolled and intercritically-annealed or as thermomechanically-rolled.

The direct effect of Mn, Al, and Si addition is forming sulfide, oxide or complex inclusions. In microalloyed and/or aluminium-containing steels complex carbides, nitrides, and carbonitrides are also often formed. It is well known that non-metallic inclusions affect significantly the properties of parent metal and steel welds. Depending on their composition, size and distribution, non-metallic inclusions may have a beneficial or detrimental effect on weld metal properties. Generally, non-metallic inclusions are considered to deteriorate the toughness, ductility, fatigue strength and corrosion resistance of steel products [14-20]. Large particles are especially harmful because they are often the initiation sites of both ductile and brittle fractures.

* SILESIAN UNIVERSITY OF TECHNOLOGY, INSTITUTE OF ENGINEERING MATERIALS AND BIOMATERIALS, 18A KONARSKIEGO STR., 44-100 GLIWICE, POLAND
** INSTITUTE OF WELDING, 16-18 BL. CZESŁAWA STR., 44-100 GLIWICE, POLAND
*** INSTITUTE OF NON FERROUS METALS, 5 SOWIŃSKIEGO STR., 44-100 GLIWICE, POLAND

The important problem during resistance welding and laser welding of TRIP steels can be cold cracking of welds as a result of high cooling rates between 800 and 500°C. The hardness of the weld in Si-bearing TRIP steels can be as high as 550 HV [19, 21-23]. Cretteur et al. [21] reported that the improvement of weldability of C-Mn-Si TRIP steels can be done by applying in-situ pre- and post-heat treatments. The reduction of hardness occurs after total replacing silicon by aluminium. However, Amirthalingam et al. [24] showed that in this case there is a risk of obtaining a soft ferrite zone near the fusion line.

The effect of non-metallic inclusions on mechanical properties of TRIP steels has been rarely studied so far. Han et al. [19] observed porosity in typical laser-welded 0.2C-1.5Mn-1.5Si steel. The pores reduced the elongation of the specimens subjected to a tensile test perpendicular to the weld axis. Recently, Amirthalingam et al. [25, 26] reported that a large fraction of complex non-metallic inclusions of various size forms in the fusion zone of Si-bearing and Al-bearing steels. Their analysis indicated that the identified inclusions are primarily oxides of aluminium with epitaxial enrichment of manganese and phosphorous. Up to now, there is no systematic study on a mechanism of the formation of non-metallic inclusions in thermomechanically processed steels. Additionally, a lack of knowledge is present regarding microalloyed TRIP steels.

2. Experimental procedure

The work is focused on issues related to laser welding of Si-Al type TRIP steel containing 0.24% C, 1.55% Mn, 0.87% Si, 0.4% Al, 0.03% Nb, 0.023% Ti, 0.004% S, 0.01% P, and 0.0028% N. The steel was produced by vacuum induction melting followed by casting under Ar atmosphere, hot forging and rough rolling to a thickness of about 5 mm. In order to modify non-metallic inclusions, rare earth elements (REE) as mischmetal (~50%Ce, ~20%La, ~20%Nd) were added. The steel was designed to obtain a large fraction of retained austenite and carbide-free bainite by medium-Si medium-Al concept [7-9]. Nb and Ti microadditions were used to increase strength through grain refinement and precipitation strengthening. Samples of 2 mm in thickness for welding purposes were obtained after thermomechanical rolling and controlled cooling with isothermal holding of the sheets at 350°C for 600 s [9].

Tests of laser welding were carried out in an air atmosphere using the keyhole welding technique with a solid-state laser, integrated with a robotized laser treatment system. The station is equipped with the TruDisk 12002 solid-state laser type Yb:YAG characterized by a maximum power of 12 kW [27]. Laser welding was carried out using the heat input value of 0.048 kJ/mm. Welding tests were followed by detailed metallographic investigations using light microscopy (LM) and scanning electron microscopy (SEM). A microstructural analysis was carried out in the fusion zone (FZ), in the heat affected zone (HAZ), and base metal (BM) as well. Special attention was put to identify retained austenite. Microscopic tests were carried out with a Leica MEF 4A light microscope after 3% nital etching. Morphological details of microstructural constituents were revealed with the SUPRA 25 SEM using back-scattered electrons (BSE) at an accelerating voltage of 20kV.

Non-metallic inclusions occurring in the base metal, heat-affected zone, and fusion zone were revealed on polished samples. The point and linear analyses as well as EDS mapping were carried out to assess a chemical composition and a morphology of identified particles. The quantitative point measurements of the chemical composition of particles were also carried out using the EDS technique. The analysis was done with the use of the JCXA 8230 X-ray microanalyser at the accelerating voltage of 15 kV and the current of 30 nA. Micrographs were registered using secondary electrons (SE) and back-scattered electrons (BSE) at the magnification range between 3000-4000x.

3. Results and discussion

3.1. Microstructure of the weld

Thermomechanically processed steels are characterized by high dispersion of individual phases. The investigated steel possesses also a fine-grained microstructure due to complex Nb+Ti microalloying resulting in grain refinement and precipitation strengthening [9, 23]. Figure 1 presents the microstructure of the weld. Boundaries between the base metal, heat-affected zone, and fusion zone can be clearly visible (Fig. 1a). The heat-affected zone is composed of intercritical HAZ (IC-HAZ), fine-grained HAZ (FG-HAZ), and coarse-grained HAZ (CG-HAZ), which are apparent in Fig. 1b. At higher magnification the approximate boundary between CG-HAZ and FG-HAZ is present (Fig. 1c), what is related to the temperature increase from the BM to the fusion line. The microstructure of the FZ contains columnar crystals of a lath morphology arranged perpendicularly to the weld axis (Fig. 1b, d).

A morphology of the individual microstructural constituents present in the particular zones of the weld can be identified using scanning electron microscopy. The micrograph in Figure 2a shows the microstructure of the base metal. The matrix of the BM is composed of flattened fine-grained ferrite containing bainite and retained austenite inclusions. Fine blocky retained austenite grains located at ferrite boundaries and interlath retained austenite (A) located in bainitic regions are thermally stable whereas the largest γ grains transformed partially into martensite upon cooling forming MA constituents. The amount of retained austenite amounts to about 15% [9, 27]. The intercritical heat-affected zone corresponds to the temperature region between A_{c1} and A_{c3} critical temperatures. The increase in the amount of bainitic-martensitic lath constituents can be observed in Fig. 2b. Retained austenite has an interlath morphology in this zone forming martensite-bainite-austenite (MBA) constituents. The partitioning of C from polygonal and bainitic ferrite to γ phase fosters stabilization of the retained austenite.

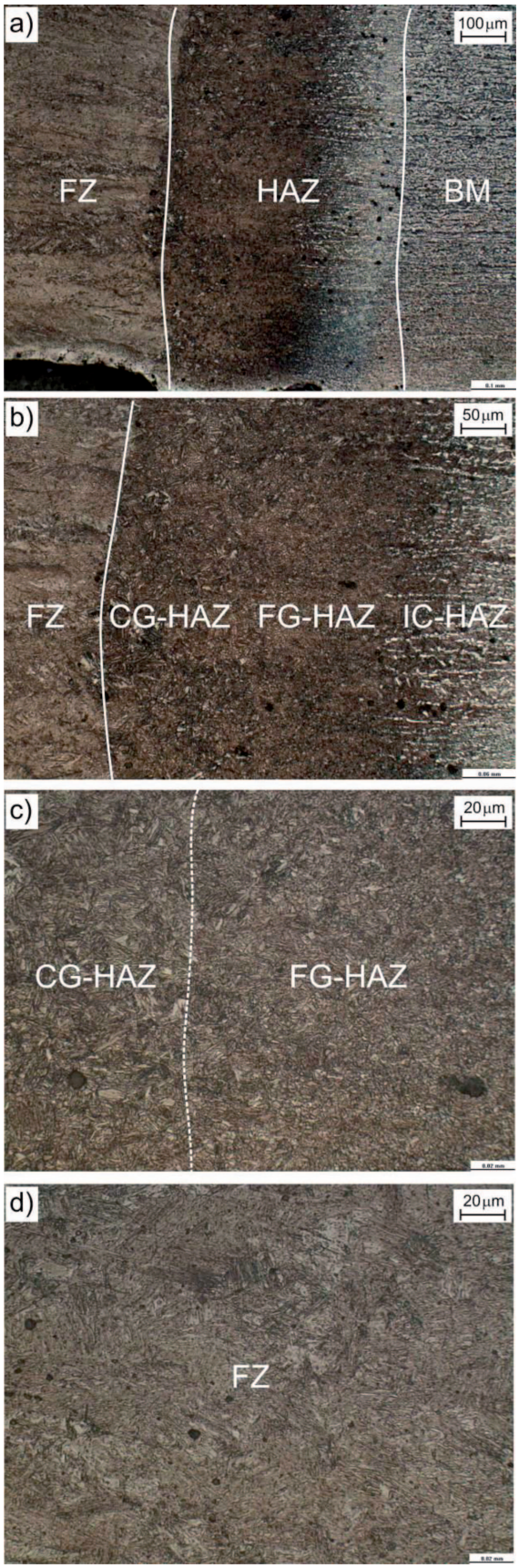

Fig. 1. Microstructure of the weld showing boundaries between base metal (BM), heat-affected zone (HAZ), and fusion zone (FZ) (a), coarse-grained CG-HAZ, fine-grained FG-HAZ, intercritical IC-HAZ and FZ (b), CG-HAZ and FG-HAZ (c), and the lath microstructure of the FZ (d)

The microstructure of the HAZ is composed of martensitic-bainitic (MB) constituents (Fig. 2c). A small retained austenite amount of the interlath morphology can be also revealed. The size of the laths in the HAZ increases along with the decreasing distance from the fusion line, which is dependent on the heating temperature of steel during welding (Fig. 1c). A relatively small fraction of retained austenite is due to the lack of ferrite and resulting carbon partitioning from ferrite into austenite. The interlath retained austenite is also present in the microstructure of the fusion zone (Fig. 2d). Amirthalingam et al. [24] studied the variation in retained austenite transverse to the weld line in the 0.2-1.6Mn-1.1Al-0.3Si GTA-welded samples. The results showed that the FZ contains from 6 to 8 vol.% of retained austenite depending on the thermal history of the samples. The approximate interlath retained austenite fraction in the FZ of the investigated laser-welded samples can be estimated as 5%. It is in good agreement with the data given in [24]. The fast cooling rate after laser welding leads to martensitic-bainitic regions as a major structural constituent. Moreover, a large number of spherical inclusions are present, which will be characterized in detail in the next chapters.

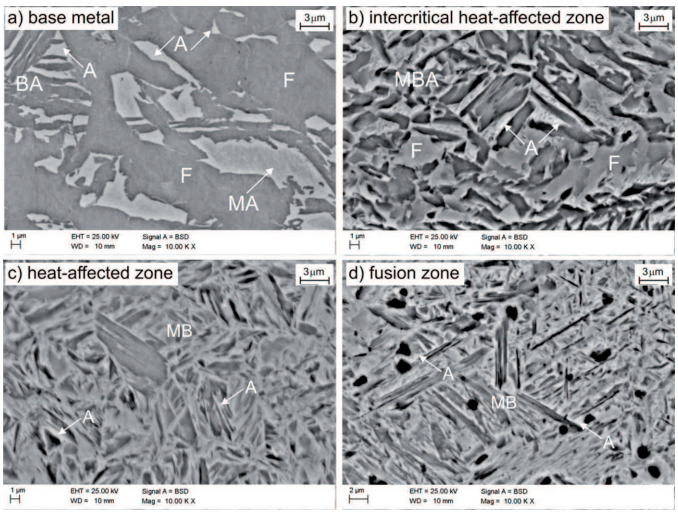

Fig. 2. Microstructure of the base metal (a), intercritical heat-affected zone (b), heat-affected zone (c), and fusion zone containing numerous non-metallic inclusions (d); F – ferrite, A – retained austenite, BA – bainitic-austenitic constituents, MA – martensitic-austenitic constituents, MBA – martensitic-bainitic-austenitic constituents, MB – martensitic-bainitic constituents

3.2. Distribution of non-metallic inclusions

The presence of elements with a strong chemical affinity for oxygen (Al, Mn, Si) in the investigated steel and the lack of a protecting atmosphere result in forming a large number of non-metallic inclusions in the fusion zone. A clear boundary between the FZ and HAZ can be also identified in Fig. 3a because the amount of non-metallic inclusions in the HAZ and BM is significantly smaller (Fig. 3b).

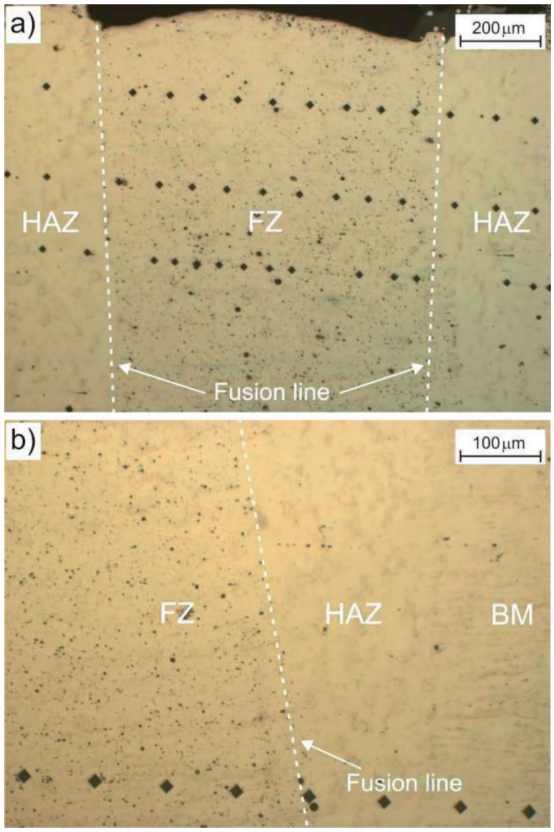

Fig. 3. Distribution of non-metallic inclusions in the fusion zone FZ (a) and near the fusion line (b) in the polished sample

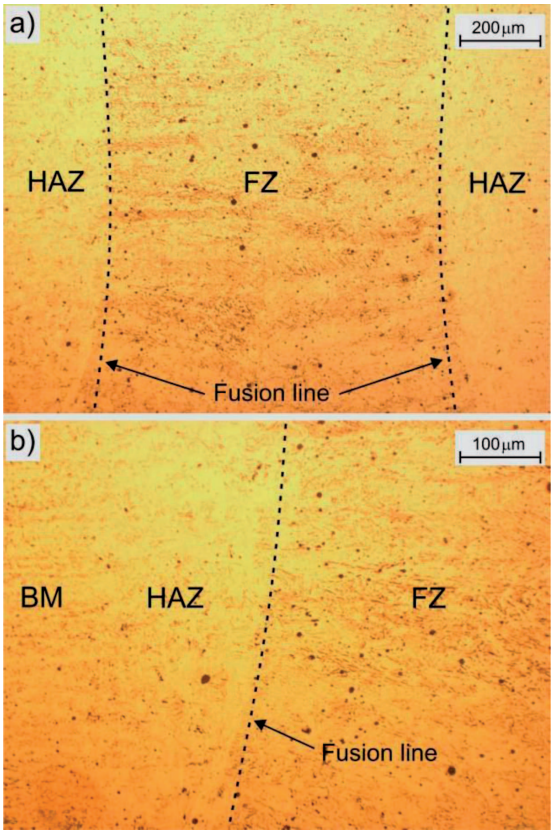

Fig. 4. Distribution of non-metallic inclusions in the fusion zone FZ (a) and near the fusion line (b) in the sample slightly etched using nital

Han et al. [19] observed some porosity in laser-welded 0.2C-1.5Mn-1.5Si steel samples. Pores were present at a low welding speed under Ar atmosphere but their amount siginificantly decreased with increasing welding speed or using Ar+He mixed gas. The micrographs in Figure 2d can also suggest the presense of porosity in investigated samples. However, it is the typical impression caused by using back-scattered electrons in SEM. The results registered by the use of secondary electrons and EDS mapping indicated that the identified particles are non-metallic inclusions.

Amirthalingam et al. [25] observed that numerous non-metallic inclusions are formed in the fusion zone of both high-Al and high-Si TRIP steels. Their results of the gas tungsten arc (GTA) welding showed that non-metallic inclusions decorated the columnar grain boundaries of the FZ near the HAZ whereas the particles were mainly located inside the equiaxed grains at the centre of the FZ. It is obvious that the penetration width during laser welding is much smaller when compared to the GTA. Therefore, the uniform distribution of non-metallic inclusions in the whole fusion zone can be apparent in Figs. 3 and 4. The slightly etched micrograph in Figure 4 indicates that the particles are not preferentially distributed along grain boundaries but they are located randomly throughout the FZ. The limited time for the particles' growth during welding and cooling results in their small size. The number of non-metallic inclusions in the HAZ and BM is much smaller than that of the FZ. They are also uniformly distributed in the sample (Figs. 3 and 4).

3.3. Non-metallic inclusions in the base metal and heat-affected zone

The investigated steel is characterized by a high metallurgical cleanliness related to low contents of sulphur, phosphorus, and gases, i.e., 0.004% S, 0.01% P, 0.0028% N, and 0.0006% O. The high cleanliness is directly reflected in a low fraction of non-metallic inclusions (Figs. 3 and 4). Some aggregates of elongated inclusions can be incidentally identified in Fig. 3b. However, the majority of particles in the BM and HAZ are small, mostly globular inclusions.

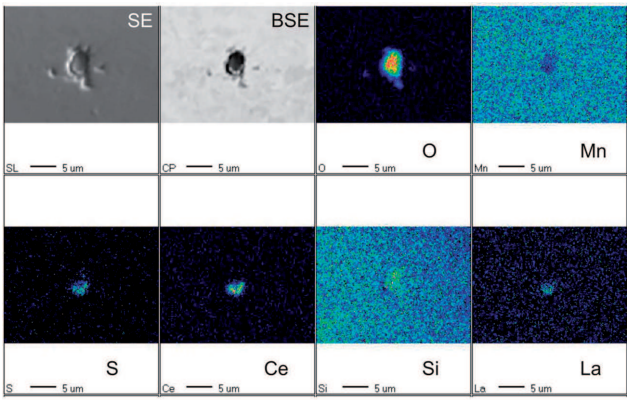

Fig. 5. Elemental mapping of the globular oxysulfide partially modified by Ce and La in the BM zone

The detailed analysis performed elsewhere [28] revealed that the average size of inclusions is equal to 19 μm^2 and the aspect ratio amounts to about 1.5. It means that the non-metallic inclusions have a reduced tendency to elongate.

Therefore, they should not detrimentally affect the toughness of the steel sheets due to anisotropy effects.

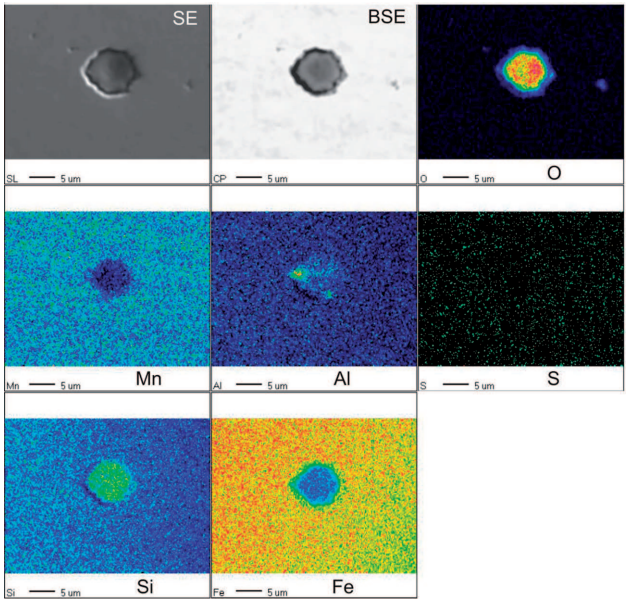

Fig. 6. Elemental mapping of the globular oxide containing Si and Al in the heat-affected zone

The result of the interaction between rare earth elements and basic alloying elements is obtaining complex oxysulfides with the low susceptibility for plastic deformation during thermomechanical rolling. Figure 5 shows a typical, fine, globular particle occurring in the base metal. The elemental mapping reveals clear that it is the complex oxysulfide containing O, S, Si, Ce, and La. Taking into account the high chemical affinity of REE to oxygen and sulphur and the high melting points of their compounds [15, 28] they are presumably formed directly after their adding into the liquid bath. The melting points of oxides, sulfides or oxysulfides formed by REE are higher compared to the melting points of MnS (1539°C) and Al_2O_3 (2030°C). Hence, Ce and La displace Mn in sulfide inclusions and Mn and Si in oxide particles, forming phases of higher thermal stability and hardness. It should be noted that manganese is replaced entirely and silicon only to a limited extent (Fig. 5). Some of the inclusions in the BM and HAZ are not modified by REE. As the example, Figure 6 shows elemental mapping of the globular oxide containing Si and Al in the HAZ.

3.4. Non-metallic inclusions in the fusion zone

Due to the high chemical affinity of Al, Si, and Mn for oxygen from the air, numerous oxides are formed in the fusion zone. Figure 7 presents non-metallic inclusions of various size in the FZ composed of martensitic-bainitic laths and interlath retained austenite (RA). Moreover, the linear distribution of the content of individual elements along line 1 is included (Fig. 7b). It is clear that the identified particle with a diameter smaller than about 2 μm is aluminium oxide. The concentrations of oxygen and aluminium increase gradually reaching maximum values in a middle of the particle.

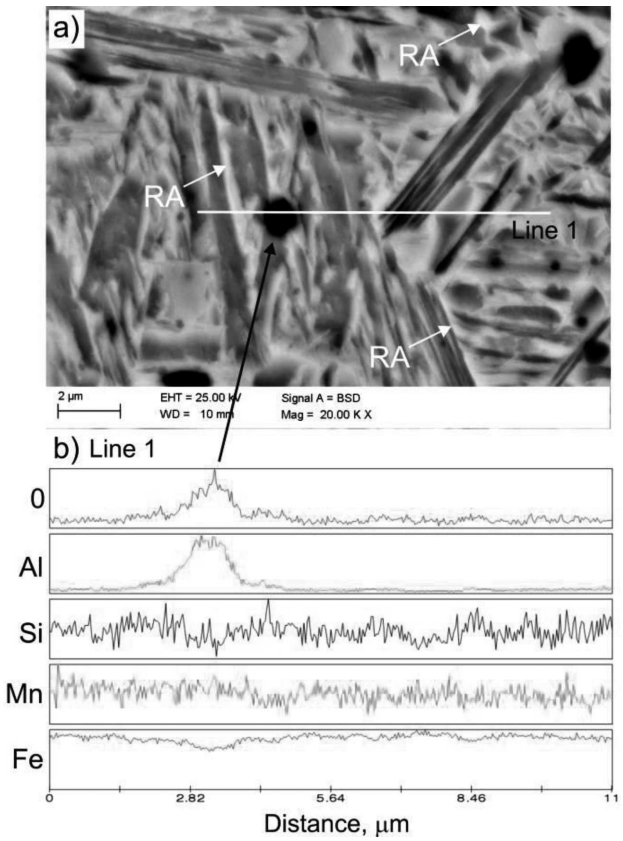

Fig. 7. Non-metallic inclusions in the FZ composed of martensitic-bainitic laths and interlath retained austenite RA (a) and linear distribution of the content of individual elements along line 1 (b)

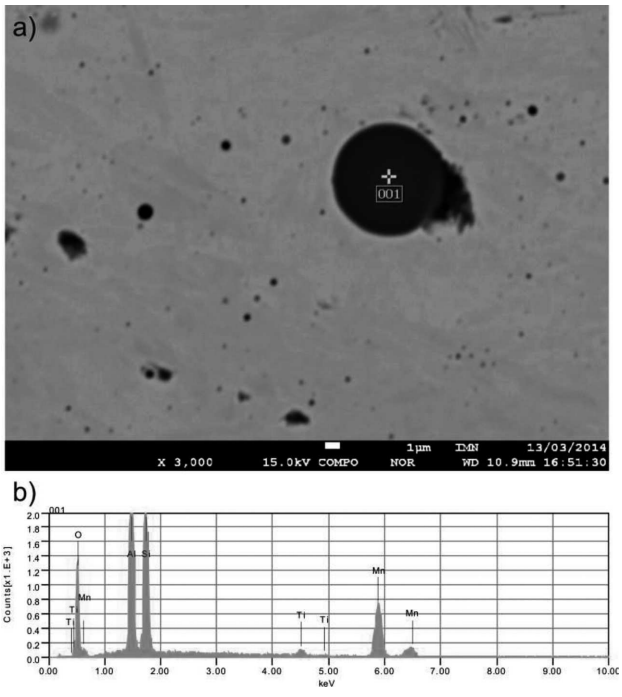

Fig. 8. The globular oxide containing Al, Mn, Si, and small amount of Ti; a – view of the large inclusion and numerous smaller particles, b – spectrum of the large inclusion from the point 1

The larger globular complex oxide with a diameter of about 7 μm can be seen in Fig. 8. Spectrum lines indicate the presence of O, Al, Si, and Mn. The identification of small

amounts of Ti microaddition was also possible. There are no spectral lines from sulphur. Additionally, numerous small particles with a size smaller than about 2 μm are statistically arranged in the steel weld. A more detailed elemental mapping in Fig. 9 confirms a complex character of the large inclusion containing Al, Si, and Mn. Moreover, the small particles can be identified as pure aluminium oxides because they do not contain manganese or silicon. Another examples of globular oxide particles can be seen in Fig. 10. The energy dispersive spectroscopy analysis of inclusions indicates that these particles are complex or pure oxides.

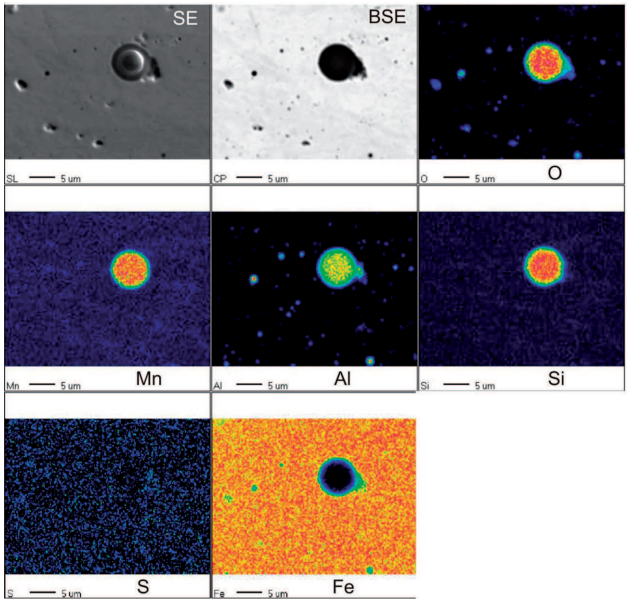

Fig. 9. Elemental mapping of the globular oxides of various sizes located in the FZ

The quantitative analysis of the chemical composition of inclusions (Table 1) marked as points 001 and 002 in Fig. 10 clearly indicate that the large particle is composed of Al, Si, and Mn. Al has stronger chemical affinity for oxygen than silicon and manganese. For this reason the content of Al in the inclusion is much higher when compared to Si and Mn (Table 1). Moreover, the quantitative analysis of the smaller particle in Fig. 10 (marked as the 002 point) reveals that the Al content doubled whereas the contents of Mn and Si are close to 0. The distribution maps of elements in Fig. 11 show that the large particle can be identified as the complex oxide containing primarily Al and smaller amounts of Si and Mn, whereas small particles correspond to pure aluminium oxides. The same dependence was observed in Fig. 9. The limiting size between complex and pure oxides seems to be about 2 μm.

Similar oxide-type inclusions in the FZ were identified by Amirthalingam et al. [25, 26] in high-Al and high-Si TRIP steels. They also found that particles containing aluminium are greater in size than inclusions containing silicon, which is due to the higher temperature of Al_2O_2 formation. Their EDS analyses revealed that the aluminium oxide forming already in the liquid weld pool is followed by formation of silicon oxide, and subsequent epitaxial enrichment of the inclusion in MnS below the solidification temperature takes place. In contrast, the inclusions forming in the investigated steel do not contain sulphides due to the fast cooling rates characteristic for laser welding when compared to the GTA welding. The fast cooling rate is also a reason why small pure aluminium oxides are smaller in size than complex oxide particles containing Al, Si, and Mn. The presence of Ti in Figure 11 suggests that this element forming very stable oxides can also stimulate oxides' forming.

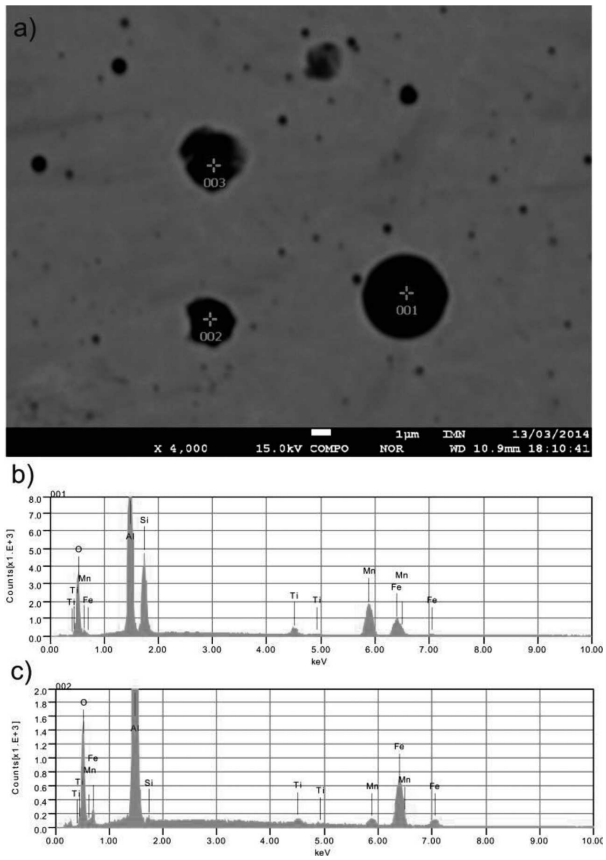

Fig. 10. The large complex oxide containing Al, Si, Mn, and Ti and smaller pure aluminium oxide inclusions; a – view of the large inclusion and numerous smaller particles, b – spectrum of the large inclusion from the point 1, c – spectrum of the smaller inclusion from the point 2

TABLE 1

Chemical composition of the inclusions marked in Fig. 10 determined using EDS technique

Point 1	wt. %	at. %
O	38.1	58.5
Al	20.0	18.2
Si	10.4	9.1
Ti	1.9	1.0
Mn	18.9	8.5
Fe	10.7	4.7
Point 2	wt. %	at. %
O	38.4	56.5
Al	38.0	33.2
Si	0.6	0.5
Ti	0.8	0.4
Mn	2.2	0.9
Fe	20.1	8.5

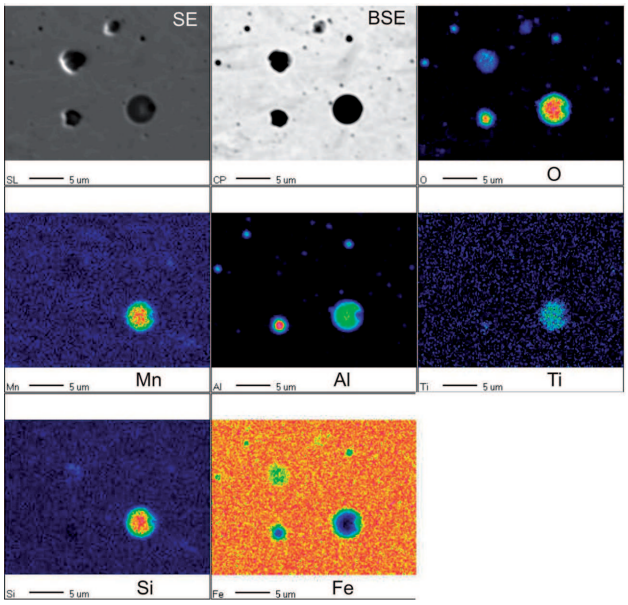

Fig. 11. Elemental mapping of the globular complex and pure oxides of various sizes located in the FZ

4. Conclusions

A detailed identification of non-metallic inclusions present in the base metal, heat-affected zone, and especially in the fusion zone of laser-welded Si-Al steel containing Ti and Nb microadditions was carried out. The BM and HAZ revealed the presence of oxysulfide or oxide inclusions partially modified by rare earth elements. They are fine particles of a globular shape and a low tendency for plastic deformation during thermomechanical rolling. Uniformly distributed non-metallic inclusions identified in the fusion zone have a globular shape and a maximum diameter of about 7 μm. The complex oxides containing Al, Si, Mn, and Ti are characterized by largest sizes whereas the content of Al increases and the contents of Mn and Si decrease with reducing particle's diameter. Numerous pure aluminium oxides are smaller than 1 μm due to a fast cooling rate typical for laser welding. On the one hand non-metallic inclusions deteriorate the weld quality, on the other hand the welding efficiency reduces significantly when a protecting atmosphere is applied. Therefore, further research concerning the effect of non-metallic inclusions on mechanical properties of welds is needed. The microstructure of the FZ is composed of martensitic-bainitic laths and inter-lath retained austenite.

REFERENCES

[1] J. Senkara, Weld. Int. **3**, 184 (2013).
[2] M. Weglowski, S. Stano, K. Krasnowski, M. Lomozik, K. Kwiecinski, R. Jachym, Mater. Sci. Forum **638-642**, 3739 (2010).
[3] M. Pernach, K. Bzowski, R. Kuziak, M. Pietrzyk, Mater. Sci. Forum **762**, 699 (2013).
[4] M. Adamczyk, D. Kuc, E. Hadasik, Arch. Civ. Mech. Eng. **8**, 3, 5 (2008).
[5] A. Kokosza, J. Pacyna, Arch. Metall. Mater. **55**, 4, 1001 (2010).
[6] S. Wiewiorowska, Arch. Metall. Mater. **58**, 2, 573 (2013).
[7] J. Jung, S.J. Lee, S. Kim, B.C. De Cooman, Steel Res. Int. **82**, 857 (2011).
[8] D. Krizan, B.C. De Cooman, Steel Res. Int. **79**, 7, 513 (2008).
[9] A. Grajcar, K. Radwanski, H. Krzton, Solid State Phenom. **203-204**, 34 (2013).
[10] A. Lisiecki, Diode laser welding of high yield steel, Proceedings of SPIE, Laser Technology 2012: Application of Lasers, **8703** (2013), DOI: 10.1117/12.2013429.
[11] M. Opiela, A. Grajcar, Arch. Civ. Mech. Eng. **12**, 4, 427 (2012).
[12] T. Sleboda, K. Muszka, J. Majta, P. Hale, R.N. Wright, J. Mater. Proc. Tech. **177**, 1-3, 461 (2006).
[13] J. Gorka, Influence of welding thermal cycling on the join properties of S 700MC steel treated using thermomechanical method, in: J.F. Silva Gomes, M.A.P. Vaz (Eds.), Proc. of 15th International Conference on Experimental Mechanics, Article no. UNSP 2980 (2012).
[14] H.K.D.H. Bhadeshia, Recent Trends in Welding Science and Technology, ASM International, Metals Park, Ohio 1990.
[15] T. Gladman, The Physical Metallurgy of Microalloyed Steels, The Institute of Materials, The University Press, Cambridge 1997.
[16] D.S. Sarma, A.V. Karasev, P.G. Jonsson, ISIJ Int. **49**, 7, 1063 (2009).
[17] B. Zorc, M. Imamovic, L. Kosec, B. Kosec, A. Nagode, Mater. Tehnol. **48**, 1, 149 (2014).
[18] S.S. Babu, S.A. David, ISIJ Int. **42**, 12, 1344 (2002).
[19] T-K. Han, S.S. Park, K-H. Kim, C-Y. Kang, I-S. Woo, J-B. Lee, ISIJ Int. **45**, 1, 60 (2005).
[20] E. Tasak, Weld. Int. **25**, 12, 938 (2011).
[21] L. Cretteur, A.I. Koruk, L. Tosal-Martinez, Steel Res. **73**, 314 (2002).
[22] R.S. Sharma, R. Molian, J. Mater. Proc. Tech. **211**, 1888 (2011).
[23] A. Grajcar, M. Różański, S. Stano, A. Kowalski, B. Grzegorczyk, Adv. Mater. Sci. Eng. **2014**, 8 pages (2014), DOI: 10.1155/2014/658947.
[24] M. Amirthalingam, M.J.M. Hermans, L. Zhao, I.M. Richardson, Metall. Mater. Trans. A **41**, 431 (2010).
[25] M. Amirthalingam, M.J.M. Hermans, I.M. Richardson, Metall. Mater. Trans. A **40**, 901 (2009).
[26] M. Amirthalingam, M.J.M. Hermans, I.M. Richardson, Adv. Mater. Res. **89-91**, 23 (2010).
[27] A. Grajcar, M. Różański, S. Stano, A. Kowalski, J. Mater. Eng. Perform., (2014) DOI: 10.1007/s11665-014-1118-1.
[28] A. Grajcar, Rudy i Metale Nieżelazne **55**, 3, 143 (2010) in polish.

Received: 20 March 2014.